

Disclosing the Impact of Local Host-Emitter Interactions on Donor-Acceptor Type TADF Dynamics and the Significance for Emissive Layer Design in OLEDs

Björn Ewald^{*†}, Theodor Kaiser[†], Thomas Fleischmann[†], and Jens Pflaum^{*†||}

[†] Experimental Physics VI, Julius-Maximilian University, Am Hubland, 97074 Würzburg, Germany

^{||} Center for Applied Energy Research e.V. (CAE), Magdalena-Schoch Straße 3, 97074 Würzburg, Germany

KEYWORDS. *Organic Light Emitting Diode, thermally-activated delayed fluorescence, single molecule spectroscopy, single photon source, photon correlation, organic semiconductor*

ABSTRACT: Donor-Acceptor (D-A) type thermally activated delayed fluorescence (TADF) emitters which constitute the key functional units in proposed Gen3 Organic Light Emitting Diodes (OLEDs), are sensitive to the rigidity and polarity of their local environment. In particular, the torsional freedom of the D-A dihedral angle and the excited state dipole moments of the occurring charge transfer states, condition a distribution of TADF dynamics over the emitter ensemble, concealed in standard optical spectroscopy. Here we apply spectroscopy on the single molecule level to directly access individual emitter properties, and, thus, bypass the downside of ensemble averaging. By photon correlation data and locally resolved spectral information on single D-A type TADF molecules embedded in technological relevant host materials of different polarity and rigidity, we derive host-dependent characteristics and distributions in the TADF dynamics. Those can be related to the conformational freedom and the dielectric environment imposed by the specific local host rigidity and polarity, thereby pointing out new selection criteria for host-emitter combinations in OLEDs.

Introduction

Thermally-activated delayed fluorescence (TADF) constitutes key research interest in the field of Organic Light Emitting Diodes (OLEDs), since the TADF mechanism facilitates efficient harvesting of triplet excitons by means of Boltzmann-activated up-conversion to singlet excitons in absence of heavy metals in the molecular scaffold. Hence, TADF emitters define the main innovation in so-called Gen3 OLEDs. Reverse intersystem crossing (rISC) is favored by a small energetic gap ΔE_{ST} between the excited singlet state S_1 and the triplet T_1 manifold. Basic molecular structures consist of a donor (D) and acceptor (A) unit linked via a bridging element, alleviating the spatial overlap of the highest occupied molecular orbital (HOMO) and the lowest unoccupied orbital (LUMO) and thus minimized electronic exchange interaction.^[1-3] The S_1/T_1 states of a D-A emitter constitute charge transfer (CT, 1CT and 3CT) excitons of different spin multiplicity and with inherent excited state dipole moment. A third localized excited triplet state (3LE) energetically close to the 3CT state mediates wavefunction intermixing with the 1CT state and concomitant spin-orbit coupling (SOC), hence, supporting effective ISC and rISC.^[4-8] The dihedral angle between the D/A units affecting the HOMO-LUMO wavefunction overlap plays the dominating role in reducing ΔE_{ST} .^[9-14] Considering Fermi's golden rule, the reverse intersystem crossing rate k_{rISC} exhibits the following

proportionality (Equation 1) to the transition matrix element $\langle S_1 | \hat{H}_{SOC} | T_1 \rangle$ of SOC between S_1 and T_1 and to the energy gap ΔE_{ST} .^[8, 15]

$$k_{rISC} \propto \langle S_1 | \hat{H}_{SOC} | T_1 \rangle \cdot e^{-\frac{\Delta E_{ST}}{k_B T}} \quad (1)$$

Here k_B is the Boltzmann constant and T the temperature. Beside the intrinsic rate dynamics controlled by the molecular motif, TADF dynamics is susceptible to the local environment and therefore is heavily influenced by the local dielectric and steric properties of the complementary host material as highlighted in Figure 1 a.^[16-21] More specifically the energetic arrangement of 1CT , 3CT and 3LE states is directly targeted by the host polarity, while the host rigidity imposes constraints to the conformational freedom along the dihedral angle thereby indirectly affecting the energy landscape and the SOC. This results in a distribution TADF dynamics across the individual molecules which are sensitive to their specific local environment. Disclosing such dynamic distributions would allow for a more comprehensive understanding of TADF emission on molecular length scales, including its dependence on the local properties of the complementary host and, thus, to access the role of the microscopic energetic and dynamics on the macroscopic behavior of TADF-based OLEDs. In contrast, the local dependence and distribution of TADF properties are concealed in state-of-the-art ensemble techniques, particularly in

temperature dependent transient photoluminescence.^[22] Kelly et al.^[23] have pinpointed this limitation and evolved a Laplace transform fitting routine to uncover distributions of k_{rISC} in ensemble measurements.

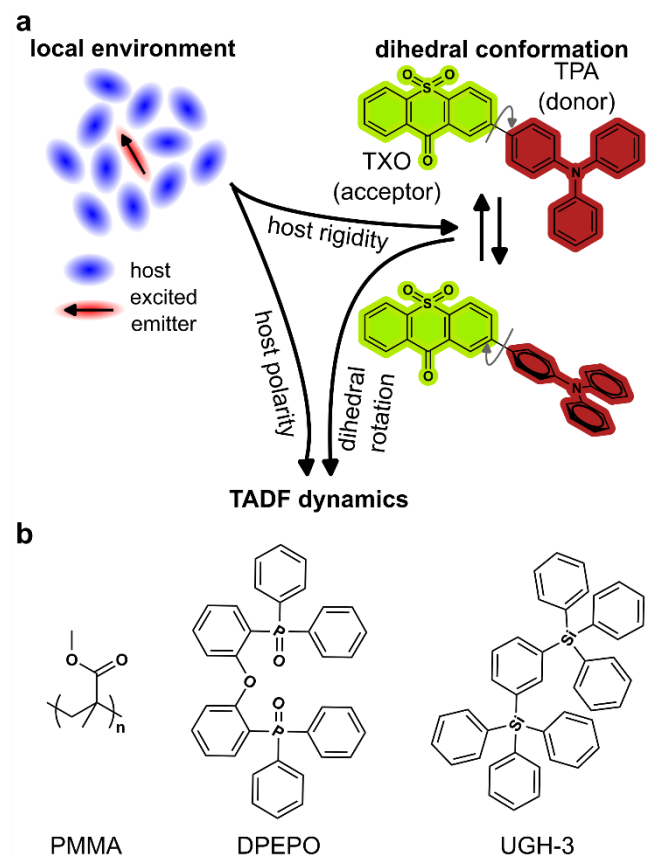


Figure 1. Conceptual design of the single molecule study. (a) Illustration of the impact of the local host environment on the singlet-triplet dynamics of the D-A type TADF emitter TXO-TPA. The quadrilateral relationship between host polarity, host rigidity, dihedral rotation and TADF dynamics is highlighted by black arrows. Single molecule spectroscopy allows for investigation of the specific and local host environment without averaging over individual emitter molecules. (b) Molecular structures of the host materials applied for the single molecule study. PMMA and DPEPO are both amorphous host materials with DPEPO exhibiting a high polarity. UGH-3 is a crystalline/rigid host with low polarity.

In contrast, we utilize single molecule spectroscopy as experimental tool to directly access individual and host specific TADF dynamics, thereby bypassing the loss of information caused by ensemble averaging. The ability of single photon techniques to identify emission mechanisms and excitonic processes has been demonstrated in various studies^[24-34] but, to best of our knowledge, has never been used to relate single molecule TADF emission to host rigidity and polarity.

Here, we systematically examined the impact of host rigidity and polarity by doping TXO-TPA (Figure 1 a, right) into the wide band gap materials poly(methylmethacrylate) (PMMA), Bis[2-(diphenylphosphino)phenyl]etheroxide (DPEPO) and 1,4-bis(triphenylsilyl)benzene (UGH-3) (Figure 1 b). Whereas by their disordered, flexible nature, PMMA and DPEPO are expected to facilitate an almost

unhindered rotation of the dihedral angle, the crystalline nature of UGH-3 is expected to restrict the dihedral rotation and vibrational freedom in TXO-TPA. Moreover, DPEPO constitutes a highly polar environment in relation to PMMA and UGH-3. Rigidity and polarity effects on the TADF dynamics are systematically investigated by performing photon correlation experiments on a mean of at least 10 independent single molecules for each host-emitter combination. For comparability reasons intensity histograms, antibunching and bunching characteristics are recorded within the same lifetime cycle, while host dependent vibronic coupling is investigated in a separate experiment by recording single molecule photoluminescence (PL) spectra. Importantly, we not simply disclose host-emitter interactions on the single molecule level, but in addition build a bridge to ensemble properties and application-oriented OLED performance.

Results and Discussion

Spectral Emission. To derive hosting effects on the vibrational and conformational freedom of TXO-TPA, which we will reconsider for the interpretation of photon correlation data, we launch our study with the discussion of single molecule PL spectra. Moreover, the analysis of PL spectra is the most instructive way for highlighting the capabilities of single molecule spectroscopy to scientists not familiar with the method. In Figure 2, representative single molecule spectra from three individual TXO-TPA molecules for each host material, are depicted. The associated ensemble PL at emitter concentrations seven orders of magnitude above single molecule concentrations is shown for comparison. An emitter dilution of 10^{-8} wt% within the respective host thin films of 100 nm thickness, corresponds to a mean in-plane spacing between individual TXO-TPA molecules of at least $1.5 \mu\text{m}$, which exceeds the diameter of the confocal excitation volume by a factor of not less than two. Complementary host thin films with a TXO-TPA concentration of 10^{-1} wt%, reflect the concentration regime commonly applied in ensemble measurements of TADF emitters. All PL spectra were measured at 532 nm continuous wave (cw) excitation and in case of the single molecule measurements at $300 \mu\text{W}$ excitation power. In the emitter ensemble, TXO-TPA features a broad and structureless PL spectrum centered around 1.99 eV in PMMA, 1.95 eV in DPEPO and 2.05 eV in UGH-3. The spectral position in a TADF ensemble is usually related to the average dielectric constant of the host material. The ^1CT state of TXO-TPA is stabilized with respect to the S_0 ground state in a polar host material. In our case, DPEPO may enforce a bathochromic shift of the mean TXO-TPA PL in relation to the non-polar UGH-3 host, due to the high polarity of the phosphine oxide group. With the PMMA host exhibiting a medium polarity, the spectral position of the TXO-TPA ensemble PL follows the polarity sequence of the host materials. The spectral width of the TXO-TPA ensemble spectra, estimated from the full width at half maximum (FWHM), is ranging from 0.38 eV in PMMA, to 0.39 eV in DPEPO and to 0.41 eV in UGH-3. The vibronic fine structure is averaged out in the ensemble PL and the host specific vibronic coupling, is in general not considered in the interpretation of TADF ensemble data.

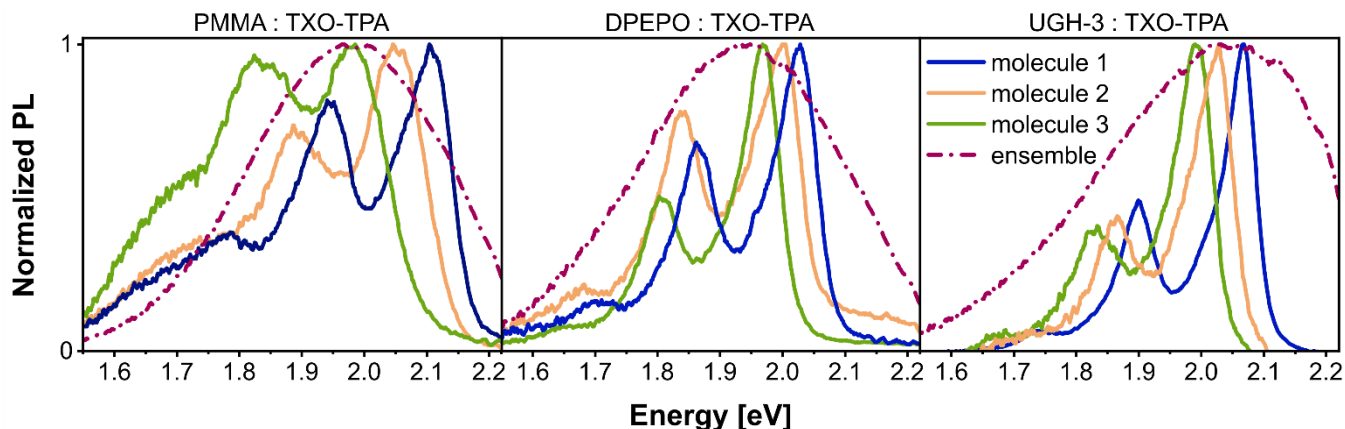


Figure 2. Normalized single molecule photoluminescence (PL) spectra of TXO-TPA dispersed in PMMA, DPEPO and UGH-3 (from left to right) at ultralow concentrations of 10^{-8} wt%. Representative PL spectra of three individual single molecules are shown for each host-guest combination. The associated ensemble PL spectra at emitter concentrations of 10^{-1} wt% are depicted for comparison in dash-dot purple lines. All single molecule measurements were carried out at 532 nm excitation wavelength and $300 \mu\text{W}$ excitation power

In contrast, the single molecule PL spectra directly disclose a distinct vibronic progression, which is caused by the 0-0, 0-1, 0-2 and 0-3 transitions between the ^1CT excited state and the S_0 ground state. The ensemble spectrum can be understood as the envelope of multiple PL spectra from individual molecules, which each experience a specific local host environment. The variation in spectral shape and position over individual TXO-TPA molecules for each host material, is a clear hint to the impact of local host-emitter interactions on TADF dynamics, which are hidden in any ensemble measurement. The vibronic main transition peaks in the single molecule PL constitute a superposition of multiple vibrational modes, as indicated by the dissymmetric line shape, which strongly deviates from Gaussian or Lorentzian line profiles. The 0-0 and 0-1 main transition are separated by 0.16 to 0.17 eV independent of the host material and the energetic spacing represents the mean vibrational mode of a single TXO-TPA molecule. Clearly host dependent, are the width of the vibronic transitions and the vibronic coupling. The average FWHM of the 0-0 transition is 0.13 eV in PMMA, 0.10 eV in DPEPO and 0.07 eV in UGH-3, which hints to the restriction of molecular vibrations in the rigid UGH-3 host in relation to DPEPO and PMMA and may also hint to a reduced freedom of dihedral rotation within a crystalline host material. A further host dependent feature is the Huang-Rhys parameter S , which characterizes the coupling of the electronic excitation to vibronic modes and can be estimated from the intensity ratio of the 0-0 and 0-1 vibrational peak by I_{0-1}/I_{0-0} .^[35] When considering a spin-vibronic mechanism in ISC and rISC dynamics a variation in the vibronic coupling may strongly alter the TADF dynamics.^[4] As indicated by the I_{0-1}/I_{0-0} ratio the mean vibronic coupling of TXO-TPA is reduced in the rigid UGH-3 host in relation to the amorphous host materials. As we will see later, this does not hamper effective rISC of TXO-TPA molecules being in a favorable conformational state in UGH-3.

Intensity Histograms. The host dependent conformational freedom of TXO-TPA has been further investigated by analysis of intensity histograms (Figure 3), which are derived from intensity time traces recorded during the photon correlation measurements. Importantly photon correlation

data and histogram data, were measured within the same lifetime cycle of a molecule. An intensity time trace with a specified binning (10 ms) can be converted into an intensity histogram by plotting the number of emitted photons within a time bin over the prevalence (frequency) of detection in various time bins. In other words, if the intensity histogram would exhibit only one dirac-like peak at 600 photons $\cdot\text{ms}^{-1}$, it signifies that 600 photons are emitted by the molecule in every time bin of the measurement period. Peak widening and the occurrence of additional peaks signifies, that the quantity of emitted photons exhibits a variation over different time bins. In this sense the intensity histogram can be grasped as a probability distribution. We emphasize, that the binning is considerably longer than the triplet lifetime of TXO-TPA ($< 100 \mu\text{s}$)^[36], therefore we do not access singlet-triplet dynamics with this method, but rather measure the occupation of a mean emissive state. In Figure 3, four representative intensity histograms from four individual TXO-TPA molecules are displayed for each host-guest combination. The probability distributions qualitatively represent the behavior over the whole set of measured molecules. In case of the amorphous PMMA and DPEPO hosts, we identify three distinct emissive states of TXO-TPA, as highlighted in Figure 3. The mean emission states (FWHM given in parenthesis) of TXO-TPA reside around 600 (48 ± 4), 460 (36 ± 5) and 350 (30 ± 2) photons $\cdot\text{ms}^{-1}$ in PMMA and around 480 (29 ± 5), 370 (33 ± 2) and 250 (22 ± 2) photons $\cdot\text{ms}^{-1}$ in DPEPO. An individual TXO-TPA molecule will occupy at least one of the three emissive states, and as shown for one exemplary molecule (black-dotted curve) may exhibit dynamic switching between two or more emissive states during the measurement period. The peaks below 200 photons $\cdot\text{ms}^{-1}$ can be assigned to the dark/dead state, where only the host material contributes to emission, and where the molecule is trapped in the triplet state or is irreversibly bleached. In contrast, for single TXO-TPA molecules embedded in UGH-3, one single and narrow emissive state is present, with a FWHM of 16 ± 2 photons $\cdot\text{ms}^{-1}$. The peak position is distributed from 100 to 350 photons $\cdot\text{ms}^{-1}$ over the measured set of individual TXO-TPA molecules.

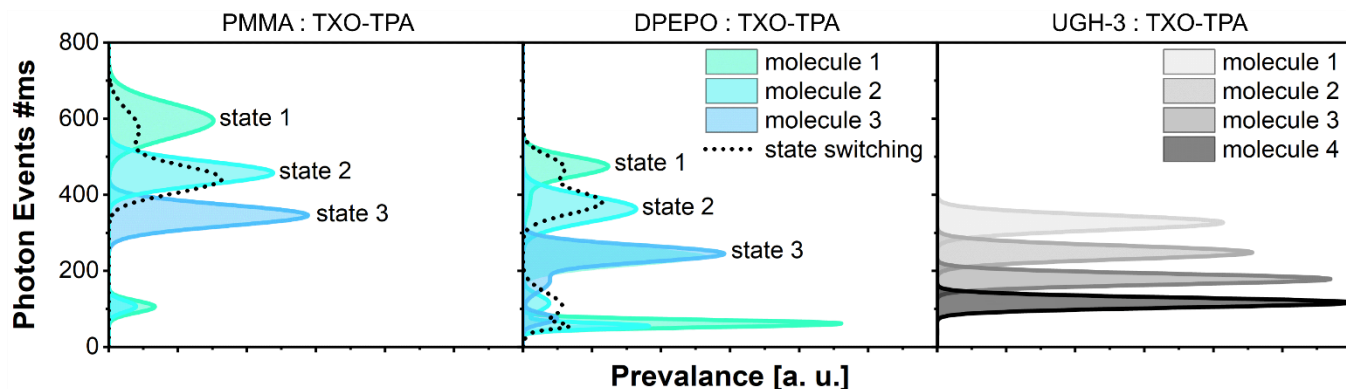


Figure 3. Intensity histograms of single TXO-TPA molecules in PMMA, DPEPO and UGH-3 (from left to right), derived from intensity time traces recorded during the photon correlation experiments with a time binning of 10 ms. The photons- ms^{-1} are applied over the prevalence, corresponding to the frequency of measuring the corresponding number of photons within a time bin. For PMMA and DPEPO representative histograms of three individual single molecules illustrating the characteristic emissive states (state 1, state 2 and state 3), and one histogram of a single molecule exhibiting pronounced switching between the emissive states (black dotted line) are presented. The peaks below 200 photons- ms^{-1} correspond to a dark or dead state, where the host material contributes to residual photon emission. For UGH-3 intensity histograms of four individual single molecules are shown, illustrating the slight brightness distribution of one distinct emissive state over different molecules. All measurements were carried out at 532 nm excitation wavelength and 300 μW excitation power.

A dynamic switching of TXO-TPA between distinct states is suppressed in the rigid UGH-3 environment, and peak widening by spectral diffusion is strongly suppressed. The FWHM, of the emissive states feature the same host related trend as observed for the width of the 0-0 transition in the spectral study. In addition, we derive a relationship between the occurrence of emissive state switching and host rigidity. The conformational freedom in the amorphous hosts PMMA and DPEPO enables a switch in emission behavior presumably associated with an alteration in between defined dihedral conformers. Peak broadening is referred to variations of the dihedral angle along the equilibrium states. The dihedral conformation in UGH-3 is restricted by the stiffness of the surrounding host, thereby defining the emissive state, and evoking a narrow peak distribution. A slight variation in brightness might be associated with variations in the absorption cross section over individual molecules. Intensity histograms allow for an intuitive understanding of rigidity effects on the single molecule level, and in combination with single photon correlation data (following section), are a powerful tool for revealing host-emitter interactions and their impact on singlet-triplet dynamics of a TADF emitter.

Single Photon Correlation. Photon correlation studies at the single molecule level allow access to the host-specific singlet-triplet dynamics of the TADF emitter by the respective antibunching and bunching characteristics as illustrated in Figure 4 a. Upon excitation of a molecule with cw excitation and detection of single photon events with two avalanche photodetectors (APDs) in a Hanbury-Brown Twiss configuration (Figure 4 a, top left) one can deduce the $g^{(2)}(\tau)$ -function (Equation 2), as the ratio of expectation values for the intensity products at time t ($I(t)$) and $t + \tau$ ($I(t + \tau)$) normalized to the square of the intensity expectation value at time t :

$$g^{(2)}(\tau) = \frac{\langle I(t) \cdot I(t+\tau) \rangle}{\langle I(t) \rangle^2} \quad (2)$$

It contains information on the probability of photon detection at time $t + \tau$ after photon detection at the other detector at time t . We have simulated, a photon correlation function (Figure 4 a, bottom) for TXO-TPA. Since an excited single molecule can only emit exactly one photon at the same time, the correlation function (Equation 2) yields zero for zero time delay resulting in photon antibunching on the nanosecond time scale in case of fluorescent emitters. For an emitter continuously excited between the S_0 and S_1 state (Figure 4 a, top right) the width of the antibunching curve provides vital information on the singlet dynamics. However, extending this scheme to the triplet manifold by ISC results in dark periods between photon bunches before the bright singlet state is repopulated again by rISC and subsequent delayed fluorescence appears (Figure 4 a, centre right). This leads to a bunching signature in the correlation function on intermediate time scales with $g^{(2)}(\tau) > 1$ and an exponentially decaying correlation amplitude with increasing time delay. Thus, the bunching signature provides direct access on the rISC versus ISC dynamics of a molecular TADF emitter.

We launch our photon correlation studies with an analysis of the single photon emission of TXO-TPA dispersed into the three respective host materials. In Figure 4 b, we depict photoluminescence intensity maps recorded for the three host-guest combinations. In PMMA, DPEPO and UGH-3 homogeneously distributed bright spots can be unambiguously discriminated from the background contribution of the host material, relating to emission from single and multiple TXO-TPA molecules with a spot size in the range of the confocal resolution down to 500 nm. The count rate at 300 μW excitation power varies from 100 to 800 counts- ms^{-1} and the host dependency has already been addressed in the previous section. The relatively high excitation power of 300 μW is a trade-off to excite TXO-TPA near saturation and to ensure an adequate correlation period without photobleaching of the single emitter.

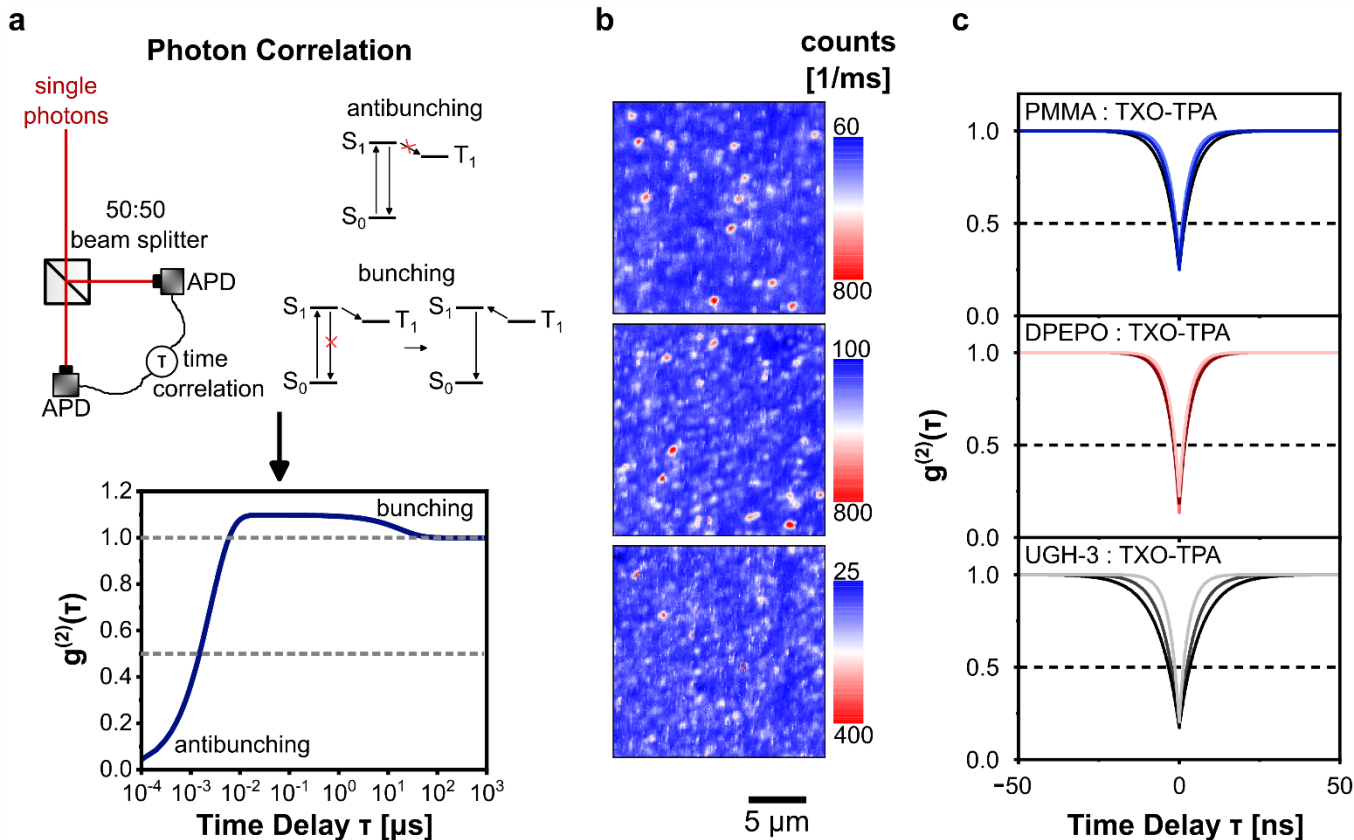


Figure 4. Photon correlation principle, photoluminescence maps and antibunching curves. (a) Single photon correlation measurements in a Hanbury-Brown Twiss geometry, composed of a 50:50 beam splitter and two avalanche photodetectors (APDs) (top left). The excitation-emission cycles for antibunching and bunching are sketched (top right). Correlation of time delays τ between single photon events yields the $g^{(2)}(\tau)$ correlation function, simulated for the TADF emitter TXO-TPA (bottom). (b) Photoluminescence intensity maps recorded on thin films with TXO-TPA dispersed on the single molecule level into PMMA, DPEPO and UGH-3 (from top to bottom). The minimum photon counts of the color bar are customized to the background contribution of the respective host material. Each map refers to an excerpt of $20 \mu\text{m} \times 20 \mu\text{m}$. (c) Corresponding $g^{(2)}(\tau)$ correlation functions of three individual TXO-TPA molecules for each host-guest combination on a time delay scale between -50 and 50 ns. For sake of clarity the mono-exponential fits of the background corrected data are depicted. The antibunching characteristics with $g^{(2)}(0) < 0.5$ clearly confirm the single photon emission of TXO-TPA in all three host materials. All measurements were carried out at 532 nm excitation wavelength and $300 \mu\text{W}$ excitation power.

In this sense, a photon correlation experiment on a TADF emitter is significantly more challenging in relation to our previously reported studies on fluorescent systems with high radiative decay constants.^[26] We note that exceptional bright spots not necessarily coincide with emission from a single TXO-TPA molecule. Explicit proof of the single photon emission nature and hence, for the presence of just one molecule in the excitation and detection spot is provided by the $g^{(2)}(0) < 0.5$ criteria at $\tau \rightarrow 0$ referred to the relation $g^{(2)}(0) = 1 - 1/N$ with N constituting the number of molecules in the focal spot contributing to emission.^[37] Antibunching curves recorded on three representative single molecules for each host-guest combination are shown in Figure 4 c. For sake of clarity, mono-exponential fits of the background corrected data are plotted. All anticorrelation curves clearly approach below 0.5 for $\tau = 0$ thus confirming the single photon emission of TXO-TPA in the host materials. In reference to Hu et al.^[38] the antibunching lifetime τ_a derived from the fit is the inverse sum of absorption rate (k_{abs}), emission rate (k_r) and non-radiative decay rate (k_{nr}) (see Equation 3):

$$g^{(2)}(\tau) = 1 - C \cdot e^{-(k_{abs} + k_r + k_{nr})\tau} = 1 - C \cdot e^{-\frac{\tau}{\tau_a}} \quad (3)$$

Here C is the magnitude of the antibunching at zero delay. k_{abs} is dependent on the excitation power and the absorption cross-section of the molecule, which leads to a deviation from standard fluorescence lifetimes. Considering the circular polarized cw-excitation and the negligible changes in absorption cross-section we relate variations in the antibunching lifetime mainly to changes in k_r and k_{nr} . The hosting effects become evident when comparing the widths of the antibunching curves for the different host materials, with UGH-3 imposing a large variation over individual TXO-TPA molecules. The lifetime distribution, measured over the whole set of individual TXO-TPA molecules in each host material leads to $\tau_{eff} = 2.7 - 4.5$ ns in PMMA, $2.8 - 3.5$ ns in DPEPO and a rather broad distribution from $2.9 - 6.7$ ns in UGH-3. We partially attribute this observation to the rigidity of the UGH-3 host hindering reorganization thereby affecting the radiative and non-radiative decay of the ^1CT exciton. We emphasize, that a pronounced bunching as observed for a small proportion of TXO-TPA molecules in UGH-3, affects the width of the antibunching. Polarity effects on the antibunching lifetime are absent, when comparing the antibunching curves for PMMA and DPEPO.

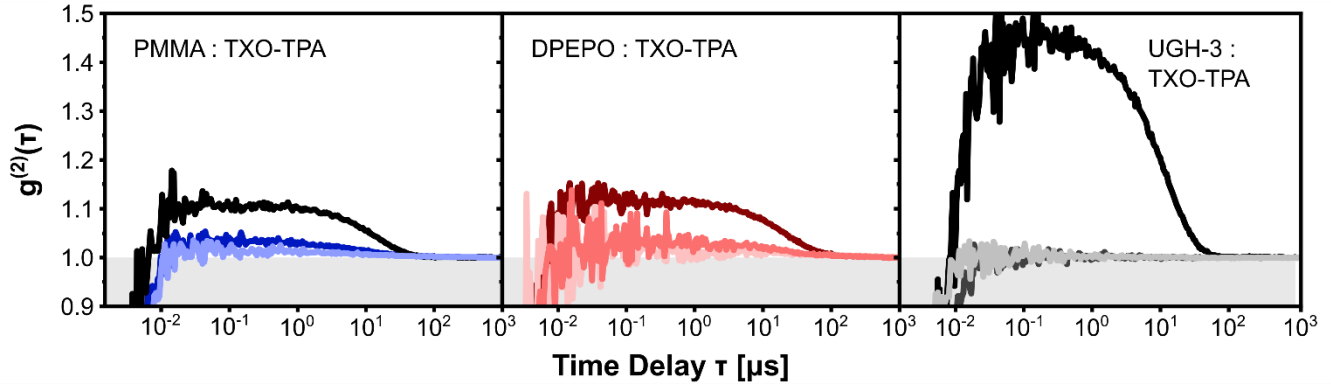


Figure 5. $g^{(2)}(\tau)$ correlation functions within a time delay of 1000 μs . For each host-guest combination measurements on three individual TXO-TPA single molecules are depicted. Bunching is present for curves approaching above $g^{(2)}(\tau) = 1$ on intermediate time scales.

As our focus, is on the host dependent singlet-triplet dynamics, we analyzed within the same lifetime cycle of the molecule, the photon bunching on intermediate delay scales. Bunching measurements of three individual single molecules for each host-guest combination are depicted in Figure 5, and reflect the variation observed for the whole set of molecules studied. Bunching is indicated for positive correlations with $g^{(2)}(\tau) > 1.0$, with the bunching amplitude A as characteristic measure for the maximum offset from non-correlated emission. We have fitted the exponential bunching decay between 0.1 μs and 1000 μs with Equation 4:

$$g^{(2)}(\tau) = 1 + A \cdot e^{-\frac{\tau}{\tau_b}} \quad (4)$$

Here A is the bunching amplitude and τ_b the decay constant quantifying the bunching duration. Magnitude and distribution of the bunching amplitude clearly constitute two host dependent features. The rigid UGH-3 host material again protrudes by its binary distribution of the bunching amplitude. TXO-TPA embedded in UGH-3 exhibits mostly negligible bunching ($A < 0.01$) or as observed for two molecular entities pronounced bunching with a distinct bunching amplitude A above 0.4. We point out that a distinct bunching amplitude in the UGH-3 host correlates with a broad width of the antibunching curve. In contrast the amorphous host materials DPEPO and PMMA provoke a slight bunching amplitude for all measured molecular entities, with a clear distribution of A between 0.01 to 0.13 (PMMA) and 0.01 to 0.11 (DPEPO). The bunching duration shows a clearly

different host dependence with τ_b of 11 μs in UGH-3, of $16 \pm 5 \mu\text{s}$ in PMMA and of $30 \pm 9 \mu\text{s}$ in DPEPO.

To derive hosting effects from the bunching amplitude distribution and the bunching length, we have modelled the correlation function of TXO-TPA based on a set of differential equations describing the relevant transitions with associated rate constants in a generic three level scheme. We refer the difference in bunching duration between the high polarity host DPEPO, the medium polarity host PMMA and the low polarity host UGH-3, to the dielectric properties of the respective host materials. The simulation shown in Figure 6 a, underlines the dependency of the bunching duration on the magnitude of k_{rISC} and k_{ISC} . We infer a polarity effect on the energetic landscape of the ^1CT , ^3LE and ^3CT state as driving factor for the enhanced bunching duration of individual TXO-TPA molecules in DPEPO. A proposed mechanism is illustrated in Figure 6 b for the medium to low polarity hosts PMMA and UGH-3 and in Figure 6 c for the high polarity host DPEPO. In a low polarity host material energetically close arrangement of ^1CT , ^3LE and ^3CT states may provide strong state mixing and concomitant SOC facilitating a fast ISC/rISC dynamics. In contrast to this, a polar host material like DPEPO may stabilize the CT states in relation to the ^3LE state thereby reducing state mixing and SOC in TXO-TPA. From the simulations we deduce that k_{rISC} and k_{ISC} of the molecular TXO-TPA entities exhibiting bunching are halved in DPEPO in comparison to PMMA and UGH-3.

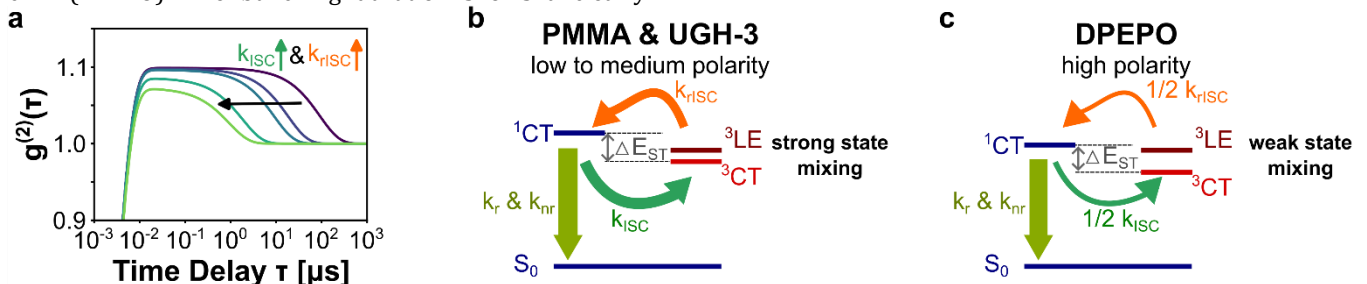


Figure 6. Simulation of singlet-triplet dynamics and proposed host polarity mechanism. (a) Simulation of correlation functions mapping a polarity-driven variation of singlet-triplet dynamics in TXO-TPA with k_{ISC}/k_{rISC} in between $10^4 \text{ s}^{-1}/10^5 \text{ s}^{-1}$ and $10^6 \text{ s}^{-1}/10^7 \text{ s}^{-1}$. (b) Schematic illustration of the singlet-dynamics imposed by the medium to low polarity hosts PMMA and UGH-3. Energetically close ^1CT , ^3LE and ^3CT states intermix and provide fast ISC/rISC dynamics by their superposition states. (c) Schematic illustration of the singlet-triplet dynamics imposed by the high polarity DPEPO host. An energetic separation of the ^3CT state from the ^3LE state results in reduced state mixing and decelerated ISC/rISC dynamics (factor 1/2) in relation to the PMMA and UGH-3 hosts.

The simulation provided in Figure 7 a, points out that the bunching amplitude of TXO-TPA is reduced with k_{rISC} approaching k_{ISC} . No bunching is observed when k_{rISC} equals k_{ISC} . Such a condition could be met, if the dihedral conformation of TXO-TPA is favoring a small energy gap ΔE_{ST} . Taking additional account of the single molecule spectra and intensity histograms, we identify rISC dynamics driven by the dihedral conformation of TXO-TPA as main influencing factor on the bunching amplitude. The amorphous host materials PMMA and DPEPO probably allow for a relatively free rotation of the dihedral angle along certain equilibrium positions, which provokes a distribution of k_{rISC} in between 10^4 s^{-1} and 10^6 s^{-1} (Figure 7 b). We emphasize, that the given rate constants should not be taken as absolute values, but rather reflect the relation of k_{rISC} to k_{ISC} in a specific host material. The rigid UGH-3 host, restricts the dihedral conformation of TXO-TPA, and apparently forces TXO-TPA into a dihedral conformation exhibiting fast rISC ($k_{rISC} = 10^6 \text{ s}^{-1}$) or exceptional slow rISC ($k_{rISC} = 10^4 \text{ s}^{-1}$), which is illustrated in Figure 7 c. Our findings support a hypothesis of Miranda-Salinas et al.^[17], who have claimed conformation-driven fast rISC dynamics of the TADF emitter TpAT-tFFO in UGH-3. Interestingly, despite the restriction of vibronic coupling and vibrational freedom visible in the PL spectra and the intensity histograms, the fast rISC dynamics in UGH-3 seems to be mainly driven by conformational effects on the energy splitting.

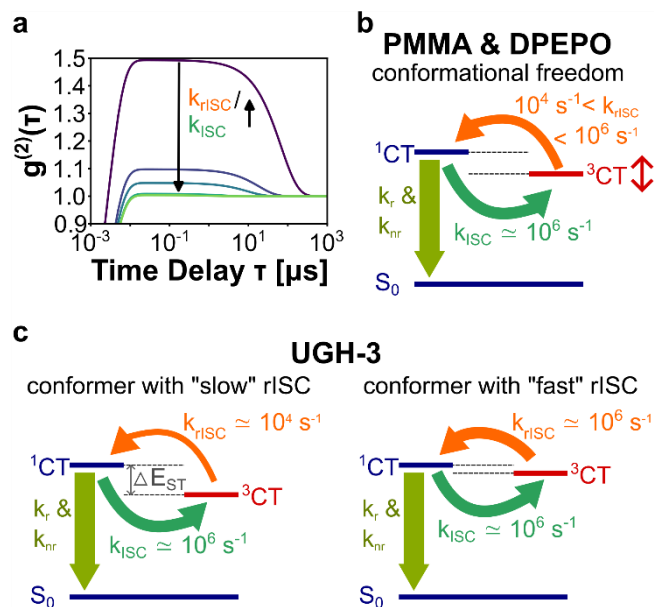


Figure 7. Simulation of rISC dynamics and proposed host rigidity mechanism. (a) Simulation of correlation functions mapping a conformation-driven variation of the rISC/ISC ratio in TXO-TPA with k_{rISC}/k_{ISC} in between 0.01 and 1. (b) Schematic illustration of the rISC dynamics imposed by the amorphous PMMA and DPEPO hosts. Freedom of dihedral rotation leads to a distribution of rISC dynamics over individual molecular entities. (c) Schematic illustration of the rISC dynamics imposed by the rigid UGH-3 host with two defined TXO-TPA conformers, one exhibiting slow rISC and one exhibiting fast rISC. We note that the given rate constants should not be taken as absolute values, but rather present the relation between k_{rISC} and k_{ISC} within the same host material.

Conclusion

We have reported on the single molecule emission of the D-A type TADF emitter TXO-TPA dispersed into the host materials PMMA, DPEPO and UGH-3 at ultralow concentrations. By means of single molecule spectra, analysis of intensity histograms and photon correlation studies, we have revealed a host dependent TADF dynamics, which can be directly related to the host polarity and rigidity. To best of our knowledge, this is the first time, that distributed properties of TADF emission have been directly accessed, without the downside of ensemble averaging. The single molecule PL spectra have revealed the host dependent freedom of molecular vibrations and vibronic coupling, which are averaged out in any ensemble measurement commonly applied. Within the rigid UGH-3 host, vibronic coupling and molecular vibrations of TXO-TPA, are drastically reduced in relation to the amorphous PMMA and DPEPO host, both visible in the reduced Huang-Rhys parameter and the spectral linewidth. Despite this and as indicated by the absence of photon bunching in the photon correlation experiments, the majority of TXO-TPA molecules, are forced into a dihedral conformation exhibiting fast rISC ($k_{rISC} = 10^6 \text{ s}^{-1}$) within the crystalline UGH-3 environment. Contrary to this, a distribution of the bunching amplitude over individual TXO-TPA molecules in amorphous DPEPO and PMMA can be related to the freedom of dihedral rotation, as indicated by three defined emissive states in the intensity histograms. This leads to distribution of k_{rISC} within PMMA and DPEPO over two orders of magnitude from 10^4 s^{-1} to 10^6 s^{-1} . In addition, the bunching length can be directly related to the polarity of the respective host material and the concomitant magnitude of k_{ISC} and k_{rISC} . We propose a reduced state mixing between the 1CT , 3CT and 3LE states by the shift in the energetic landscape imposed by the polar DPEPO environment. This leads to a reduced bunching length and concomitant halved singlet-triplet dynamics in relation to the medium polarity host PMMA. Our single molecule study thereby defines important criteria for the selection of suitable host materials in the emissive layer design of OLEDs and clearly reveals the possibility to control the magnitude and distribution of TADF dynamics in an emitter ensemble by the complementary host material.

Experimental Section

Preparation of Thin Films with Single Molecule Doping. Thin films of TXO-TPA dispersed in the host materials were prepared by spin-coating in a nitrogen glovebox system (0.0 ppm O_2 , 0.0 ppm H_2O). PMMA was purchased from Sigma Aldrich at a molecular weight of $300,000 \text{ g}\cdot\text{mol}^{-1}$. UGH-3 (Sigma Aldrich), DPEPO (Sigma Aldrich) and TXO-TPA (Lumtec) were purchased at sublimed grade. All materials were used without further purification. Prior to deposition, microscope cover slides (Karl Hecht, controlled thickness $170 \mu\text{m}$) were thoroughly cleaned by ultrasonication in double distilled water (Carl Roth) with mucasol® detergent, in double distilled water, in acetone and in isopropanol and were finally dried in a nitrogen stream. All subsequent steps were carried out under inert conditions in the glovebox system. Mixtures of the host materials and a highly diluted weight fraction of TXO-TPA ($10^{-8} \text{ wt}\%$) were

dissolved in DCM (Sigma Aldrich, spectroscopy grade) at host concentrations of 10 mg·mL⁻¹. Thin films with a thickness of 100 to 150 nm were deposited on the cover slides by spin-coating at 2000 rpm for 60 s. Thermal treatment at 70 °C for 45 minutes on a heat plate was applied for removal of parasitic solvent and concomitant crystallization of UGH-3. Afterwards parts of the sample were covered with aluminum (Al) as oxygen getter material. 120 nm of Al (Chempur, 99,9999 %) were evaporated from commercial tungsten boat sources in a glovebox-integrated vacuum chamber at rates of 2-4 Å·s⁻¹ and at a base pressure of 1·10⁻⁶ mbar. Thickness was controlled with a quartz crystal microbalance. The area for spectroscopic investigations was covered by a shadow mask. Finally, the thin films were encapsulated with glass slides and epoxy resin (Loctite EA9492). The Al covered areas reside within the encapsulation volume for thorough exclusion of residual oxygen during the single molecule measurements.

Single Molecule Spectroscopy. Single molecule photoluminescence and photon-correlation measurements were carried out at a self-made confocal microscopy setup. A 532 nm cw-laser (CNI) filtered through a spatial mode filter (Thorlabs) was used for photoexcitation. To minimize effects from orientation of molecular transition dipoles circular polarized laser light was created with a quarter and half wave plate. Excitation power densities were adjusted with a continuous grey filter wheel and measured by a commercial powermeter (Thorlabs). The samples were mounted on a piezo stage (npoint) with an overall scan range of 200x200 μm². A high numerical aperture oil-immersion objective (100x, NA = 1.49, Olympus) allows for lateral resolutions down to 300 nm. A dichroic mirror was applied in an epifluorescence configuration. In addition, the detected photoluminescence was filtered through a razor edge filter and a 550 nm longpass filter. A two-lens system with a reflective coating for additional residual laser light removal in combination with a pinhole (75 μm diameter) for background suppression was utilized. The emitted light was spectrally analyzed by a spectrometer (Princeton Instruments, Acton SP2300) in combination with a CCD camera (Pixis 400B). Two single photon avalanche diodes (Excelitas SPCM-14, QE 65 % at 650 nm, dark counts < 100 counts·s⁻¹) in a Hanbury-Brown Twiss configuration with a 50:50 beam splitter (Thorlabs), were applied for photon-correlation measurements. The $g^{(2)}(\tau)$ function of the detected photons was determined with a hardware correlation card (Becker & Hickl, DPC-230) with a time resolution of 350 ps limited by the electrical jitter of the avalanche photodiodes. Probability distributions of emitted photons per time interval were captured from intensity time traces with an integration time of 10 ms. Antibunching and bunching data as well as time trace probability distributions were recorded within the same measurement cycle for each single molecule with a total of at least 10 molecules for each host-guest combination. All antibunching data were background corrected with the intensity measured beside the single molecule spot. All measurements were carried out at 300 μW excitation power.

Simulation and modelling of correlation functions. The following set of differential equations describing the

change in population of the S₀ (p_1), S₁ (p_2) and T₁ (p_3) states was analytically solved for $p_2(\tau)$ with τ being the time delay and the rate constants k describing transitions in the generic three-state model of a TADF emitter.

$$(I) \dot{p}_1 = -k_{12}p_1 + k_{21}p_2 + k_{31}p_3$$

$$(II) \dot{p}_2 = k_{12}p_1 - (k_{21} + k_{23})p_2 + k_{32}p_3$$

$$(III) \dot{p}_3 = k_{23}p_2 - k_{31}p_3 - k_{32}p_3$$

In accordance with Hecht et al.^[39] an analytical description of the $g^{(2)}(\tau)$ correlation function was derived with the relation $g^{(2)}(\tau) = p_2(\tau)/p_2(\infty)$. The base values for the rate constants k were derived from ensemble measurements. Simulations and modelling of bunching characteristics were performed in python.

AUTHOR INFORMATION

Corresponding Authors

Björn Ewald - Experimental Physics VI, Julius-Maximilian University, Am Hubland, 97074 Würzburg, Germany

<https://orcid.org/0009-0000-7078-9252>;

Email: bjoern.ewald@uni-wuerzburg.de

Jens Pflaum - Experimental Physics VI, Julius-Maximilian University, Am Hubland, 97074 Würzburg, Germany - Center for Applied Energy Research e.V. (CAE), Magdalena-Schoch Straße 3, 97074 Würzburg, Germany

<https://orcid.org/0000-0001-5326-8244>

Email: jpflaum@physik.uni-wuerzburg.de

Author Contributions

The manuscript was written through contributions of all authors.

Notes

The authors declare no competing financial interests.

REFERENCES

- Endo, A., K. Sato, K. Yoshimura, T. Kai, A. Kawada, H. Miyazaki, and C. Adachi, Efficient up-conversion of triplet excitons into a singlet state and its application for organic light emitting diodes. *Applied Physics Letters*, 2011. 98(8).
- Goushi, K., K. Yoshida, K. Sato, and C. Adachi, Organic light-emitting diodes employing efficient reverse inter-system crossing for triplet-to-singlet state conversion. *Nature Photonics*, 2012. 6(4): p. 253-258.
- Tao, Y., K. Yuan, T. Chen, P. Xu, H. Li, R. Chen, C. Zheng, L. Zhang, and W. Huang, Thermally activated delayed fluorescence materials towards the breakthrough of organoelectronics. *Advanced materials*, 2014. 26(47): p. 7931-7958.
- Marian, C.M., Mechanism of the triplet-to-singlet upconversion in the assistant dopant ACRXTN. *The Journal of Physical Chemistry C*, 2016. 120(7): p. 3715-3721.
- Olivier, Y., B. Yurash, L. Muccioli, G. D'Avino, O. Mikhenko, J.-C. Sancho-Garcia, C. Adachi, T.-Q. Nguyen, and D. Beljonne, Nature of the singlet and triplet excitations mediating thermally activated delayed fluorescence. *Physical Review Materials*, 2017. 1(7): p. 075602.

6. Noda, H., H. Nakanotani, and C. Adachi, Excited state engineering for efficient reverse intersystem crossing. *Science Advances*, 2018. 4(6): p. eaao6910.
7. Etherington, M.K., J. Gibson, H.F. Higginbotham, T.J. Penfold, and A.P. Monkman, Revealing the spin-vibronic coupling mechanism of thermally activated delayed fluorescence. *Nature Communications*, 2016. 7(1): p. 13680.
8. Kim, J.U., I.S. Park, C.-Y. Chan, M. Tanaka, Y. Tsuchiya, H. Nakanotani, and C. Adachi, Nanosecond-time-scale delayed fluorescence molecule for deep-blue OLEDs with small efficiency rolloff. *Nature communications*, 2020. 11(1): p. 1765.
9. Weissenseel, S., N.A. Drigo, L.G. Kudriashova, M. Schmid, T. Morgenstern, K.-H. Lin, A. Prlj, C. Corminboeuf, A. Sperlich, and W. Brütting, Getting the right twist: influence of donor-acceptor dihedral angle on exciton kinetics and singlet-triplet gap in deep blue thermally activated delayed fluorescence emitter. *The Journal of Physical Chemistry C*, 2019. 123(45): p. 27778-27784.
10. Hu, T., G. Han, Z. Tu, R. Duan, and Y. Yi, Origin of high efficiencies for thermally activated delayed fluorescence organic light-emitting diodes: Atomistic insight into molecular orientation and torsional disorder. *The Journal of Physical Chemistry C*, 2018. 122(48): p. 27191-27197.
11. Wang, K., Y.-Z. Shi, C.-J. Zheng, W. Liu, K. Liang, X. Li, M. Zhang, H. Lin, S.-L. Tao, and C.-S. Lee, Control of dual conformations: developing thermally activated delayed fluorescence emitters for highly efficient single-emitter white organic light-emitting diodes. *ACS applied materials & interfaces*, 2018. 10(37): p. 31515-31525.
12. Woo, S.-J., Y.-H. Kim, and J.-J. Kim, Dihedral angle distribution of thermally activated delayed fluorescence molecules in solids induces dual phosphorescence from charge-transfer and local triplet states. *Chemistry of Materials*, 2021. 33(14): p. 5618-5630.
13. Dias, F.B., J. Santos, D.R. Graves, P. Data, R.S. Nobuyasu, M.A. Fox, A.S. Batsanov, T. Palmeira, M.N. Berberan-Santos, and M.R. Bryce, The role of local triplet excited states and D-A relative orientation in thermally activated delayed fluorescence: photophysics and devices. *Advanced Science*, 2016. 3(12): p. 1600080.
14. Etherington, M.K., F. Franchello, J. Gibson, T. Northey, J. Santos, J.S. Ward, H.F. Higginbotham, P. Data, A. Kurowska, and P.L. Dos Santos, Regio- and conformational isomerization critical to design of efficient thermally-activated delayed fluorescence emitters. *Nature communications*, 2017. 8(1): p. 14987.
15. Marian, C.M., Spin-orbit coupling and intersystem crossing in molecules. *Wiley Interdisciplinary Reviews: Computational Molecular Science*, 2012. 2(2): p. 187-203.
16. Muthig, A.M.T., O. Mrozek, T. Ferschke, M. Rödel, B.R. Ewald, J. Kuhnt, C. Lenczyk, J. Pflaum, and A. Steffen, Mechano-Stimulus and Environment-Dependent Circularly Polarized TADF in Chiral Copper (I) Complexes and Their Application in OLEDs. *Journal of the American Chemical Society*, 2023. 145(8): p. 4438-4449.
17. Miranda-Salinas, H., A. Rodriguez-Serrano, J.M. Kaminski, F. Dinkelbach, N. Hiromichi, Y. Kusakabe, H. Kaji, C.M. Marian, and A.P. Monkman, Conformational, Host, and Vibrational Effects Giving Rise to Dynamic TADF Behavior in the Through-Space Charge Transfer, Triptycene Bridged Acridine-Triazine Donor Acceptor TADF Molecule TpAT-tFFO. *The Journal of Physical Chemistry C*, 2023. 127(18): p. 8607-8617.
18. Gillett, A.J., A. Pershin, R. Pandya, S. Feldmann, A.J. Sneyd, A.M. Alvertis, E.W. Evans, T.H. Thomas, L.-S. Cui, and B.H. Drummond, Dielectric control of reverse intersystem crossing in thermally activated delayed fluorescence emitters. *Nature materials*, 2022. 21(10): p. 1150-1157.
19. Phan Huu, D.A., S. Saseendran, R. Dhali, L.G. Franca, K. Stavrou, A. Monkman, and A. Painelli, Thermally activated delayed fluorescence: polarity, rigidity, and disorder in condensed phases. *Journal of the American Chemical Society*, 2022. 144(33): p. 15211-15222.
20. Santos, P.L., J.S. Ward, P. Data, A.S. Batsanov, M.R. Bryce, F.B. Dias, and A.P. Monkman, Engineering the singlet-triplet energy splitting in a TADF molecule. *Journal of Materials Chemistry C*, 2016. 4(17): p. 3815-3824.
21. Méhes, G., K. Goushi, W.J. Potscavage Jr, and C. Adachi, Influence of host matrix on thermally-activated delayed fluorescence: Effects on emission lifetime, photoluminescence quantum yield, and device performance. *Organic Electronics*, 2014. 15(9): p. 2027-2037.
22. Haase, N., A. Danos, C. Pflumm, A. Morherr, P. Stachelek, A. Mekic, W. Brütting, and A.P. Monkman, Kinetic modeling of transient photoluminescence from thermally activated delayed fluorescence. *The Journal of Physical Chemistry C*, 2018. 122(51): p. 29173-29179.
23. Kelly, D., L.G. Franca, K. Stavrou, A. Danos, and A.P. Monkman, Laplace transform fitting as a tool to uncover distributions of reverse intersystem crossing rates in TADF systems. *The Journal of Physical Chemistry Letters*, 2022. 13(30): p. 6981-6986.
24. Bernard, J., L. Fleury, H. Talon, and M. Orrit, Photon bunching in the fluorescence from single molecules: A probe for intersystem crossing. *The Journal of chemical physics*, 1993. 98(2): p. 850-859.
25. Gernert, M., L. Balles-Wolf, F. Kerner, U. Müller, A. Schmiedel, M. Holzapfel, C.M. Marian, J. Pflaum, C. Lambert, and A. Steffen, Cyclic (amino)(aryl) carbenes enter the field of chromophore ligands: Expanded π system leads to unusually deep red emitting CuI compounds. *Journal of the American Chemical Society*, 2020. 142(19): p. 8897-8909.
26. Müller, U., P. Spent, P. Kagerer, M. Stolte, F. Würthner, and J. Pflaum, Photon-Correlation Studies on Multichromophore Macrocycles of Perylene Dyes. *Advanced Optical Materials*, 2022. 10(14): p. 2200234.
27. Muthig, A.M., M. Krumrein, J. Wieland, M. Gernert, F. Kerner, J. Pflaum, and A. Steffen, Trigonal copper (I) complexes with cyclic (alkyl)(amino) carbene ligands for single-photon near-IR triplet emission. *Inorganic Chemistry*, 2022. 61(37): p. 14833-14844.
28. Nothaft, M., S. Höhla, F. Jelezko, N. Frühauf, J. Pflaum, and J. Wrachtrup, Electrically driven photon antibunching from a single molecule at room temperature. *Nature communications*, 2012. 3(1): p. 628.
29. Nothaft, M., S. Höhla, F. Jelezko, J. Pflaum, and J. Wrachtrup, The role of oxygen-induced processes on the emission characteristics of single molecule emitters. *physica status solidi (b)*, 2012. 249(4): p. 661-665.
30. Schedlbauer, J., U. Scherf, J. Vogelsang, and J.M. Lupton, Dynamic quenching of triplet excitons in single conjugated-polymer chains. *The Journal of Physical Chemistry Letters*, 2020. 11(13): p. 5192-5198.
31. Smit, R., Z. Ristanović, B. Kozankiewicz, and M. Orrit, Reverse intersystem crossing of single deuterated perylene molecules in a dibenzothiophene matrix. *ChemPhysChem*, 2022. 23(2): p. e202100679.
32. Steiner, F., S. Bange, J. Vogelsang, and J.M. Lupton, Spontaneous fluctuations of transition dipole moment orientation in OLED triplet emitters. *The Journal of Physical Chemistry Letters*, 2015. 6(6): p. 999-1004.
33. Steiner, F., J. Vogelsang, and J.M. Lupton, Singlet-triplet annihilation limits exciton yield in poly (3-hexylthiophene). *Physical review letters*, 2014. 112(13): p. 137402.
34. Weston, K.D., M. Dyck, P. Tinnefeld, C. Müller, D.P. Herten, and M. Sauer, Measuring the number of independent

- emitters in single-molecule fluorescence images and trajectories using coincident photons. *Analytical chemistry*, 2002. 74(20): p. 5342-5349.
35. Köhler, A. and H. Bässler, *Electronic processes in organic semiconductors: An introduction*. 2015: John Wiley & Sons.
 36. Wang, H., L. Xie, Q. Peng, L. Meng, Y. Wang, Y. Yi, and P. Wang, Novel thermally activated delayed fluorescence materials—thioxanthone derivatives and their applications for highly efficient OLEDs. *Advanced Materials*, 2014. 26(30): p. 5198-5204.
 37. Lounis, B. and M. Orrit, Single-photon sources. *Reports on Progress in Physics*, 2005. 68(5): p. 1129.
 38. Hu, D. and H.P. Lu, Single-molecule triplet-state photon antibunching at room temperature. *The Journal of Physical Chemistry B*, 2005. 109(20): p. 9861-9864.
 39. Novotny, L. and B. Hecht, *Principles of nano-optics*. 2012: Cambridge university press.
-